Computers & Fluids Vol. 19, No. 2, pp. 217-230, 1991
Printed in Great Britain.
0045-7930/91 $3.00 + 0.00

ON STEADY FLOW PAST A ROTATING CIRCULAR CYLINDER AT REYNOLDS NUMBERS 60 AND 100

T. TANG AND D. B. INGHAM
DEPARTMENT OF APPLIED MATHEMATICAL STUDIES, UNIVERSITY OF LEEDS,
LEEDS LS2 9JT, ENGLAND

(Received 16 January 1990; in revised form 2 July 1990)

ABSTRACT. The unsteady flow past a rotating circular cylinder approaches a steady state after a large enough time for low Reynolds numbers. However the most recent time-dependent calculations performed by Badr et al. (*Comput. Fluids* **17**, 579; 1989) indicated that the flow does not tend to a steady state for higher Reynolds numbers, e.g. Re $= 60$ and 100. In this work steady solutions have been obtained by solving the time-independent Navier-Stokes equations for Re $= 60$ and 100 and the rotational parameter, α, in the range of $0 \leq \alpha \leq 1$. The objective is to extend the Reynolds number range for reliable data on the steady flow, particularly with regard to the lift and drag coefficients. A numerical scheme which avoids the difficulties in satisfying the boundary conditions at large distances from the cylinder is employed. Further, series expansion solutions are obtained which are valid at small values of α, but the results are found to be applicable over a wide range of values of α. The flow pattern, the surface vorticity and pressure coefficient are also presented.

1. INTRODUCTION

Fluid flow past a circular cylinder which is in steady motion, or has been started from rest, in a viscous fluid has long been of interest both experimentally and theoretically (see, e.g. Refs [1-8]). In this work we consider the flow which is generated by rotating a circular cylinder in a uniform fluid. There are two basic parameters in the problem, namely, the Reynolds number, defined as Re $= 2aU/\nu$, where ν is the coefficient of kinematic viscosity of the fluid, U the uperturbated main stream speed (in the positive x direction), a the radius of the cylinder, and the rotational parameter $\alpha = a\omega_0/U$, where ω_0 is the angular velocity with which the cylinder rotates. When $\alpha = 0$ the motion is symmetrical about the direction of translation and this situation has previously received a considerable amount of attention, e.g. Dennis and Chang [9] and Fornberg [6, 7] who both provide a comprehensive list of references.

The problem of flow past a rotating cylinder is of fundamental interest for several reasons, e.g. in boundary layer control on aerofoils [10] and the lift force experienced by the cylinder is an example of the Magnus effect and this has been used for lift enhancement [11]. Thus the general problem has been of interest both theoretically and experimentally (see, e.g. Refs [12-22]).

Although there have been a number of numerical calculations performed for the rotating cylinder problem (Refs [15-19] and [23]), steady state numerical solutions have only been obtained for Reynolds numbers up to 20. The most recent work of Badr *et al.* [16] investigated both the steady and unsteady flow past a circular cylinder and the time-dependent form of the governing equations which were formulated in terms of stream function ψ and the vorticity ω were solved. Since the correct prediction of the forces on the cylinder, particularly the lift force, was of major importance, particular attention was given to this in their paper. They found that for low Reynolds numbers the flow approaches a steady state after a sufficiently long time. However, for the higher Reynolds numbers of 60 and 100 the flow does not tend to a steady state but develops the periodic pattern of vortex shedding associated with the Karman vortex sheet. Steady solutions for Re > 20 have not yet been obtained.

In Ref. [23] the same steady problem which will be considered in this work has been investigated numerically but at low Reynolds numbers, namely Re ≤ 20. One of the main difficulties encountered in obtaining accurate numerical solutions is the satisfactory treatment of boundary conditions at large distances from the cylinder. This problem has been discussed in detail by several authors (see, e.g. Refs [6], [18] and [22]). It is clear from the results given in Ta Phuoc Loc [17] and Ingham [18] that the main physical properties of the flow, such as the lift and drag coefficients, are very much dependent, in the steady flow case, on what conditions are assumed at large distances from the cylinder. To avoid the difficulties a numerical technique was introduced by Ingham and Tang [23]. Transformations were applied to both coordinates and stream function. The numerical solutions for the full Navier-Stokes equations were obtained for Re $= 5$ and 20 and rotational parameter in the range $0 \leq \alpha \leq 3$. The calculated values of the drag and lift coefficients and the general nature of the streamline patterns were found to be in good agreement with the most recent time-dependent and time-independent calculations of Badr *et al.* [16].

In the present work we adopt the procedure used in Ref. [23] to study the steady flow past a rotating circular cylinder at higher Reynolds numbers. It is found in the present case that the numerical instabilities will give great difficulties in obtaining convergent results and particular attention should be paid to use appropriate relaxation parameters. The full Navier-Stokes solutions and the series expansion results are presented for Re $= 60$ and 100 and $0 \leq \alpha \leq 1$. Since the drag coefficient, C_D, and the lift coefficient, C_L, are of major importance and they are most sensitive to the method of solution (see, e.g. Ref. [18]) they receive particular attention in this work.

2. Mathematical Formulation

The origin is fixed at the centre of the cylinder and the positive x-axis is in the same direction as that of the translation of the cylinder. Then the non-dimensional time-independent Navier-Stokes equations, expressed in stream function Ψ and vorticity ω, take the form

$$\frac{\partial(\Psi,\omega)}{\partial(x,y)} + \frac{2}{\text{Re}}\nabla^2\omega = 0, \tag{1}$$

$$\nabla^2\Psi = -\omega, \tag{2}$$

where (x, y) are the Cartesian coordinates. It is required to solve eqns (1) and (2) subject to the boundary conditions

$$\Psi = 0, \quad \frac{\partial\Psi}{\partial r} = -\alpha, \qquad \text{on } r = 1, \quad 0 \leq \theta < 2\pi, \tag{3}$$

$$\frac{\partial\Psi}{\partial r} \to \sin\theta, \quad \frac{1}{r}\frac{\partial\Psi}{\partial\theta} \to \cos\theta, \qquad \text{as } r \to \infty, \quad 0 \leq \theta < 2\pi, \tag{4}$$

where (r, θ) are the polar coordinates which are chosen such that $\theta = 0$ coincides with the positive x-axis.

For the convenience of the numerical computation, we introduce the perturbation stream function ψ as

$$\psi = \Psi - y, \tag{5}$$

and then eqns (1) and (2) become

$$\frac{\partial(\psi,\omega)}{\partial(x,y)} - \frac{\partial\omega}{\partial x} + \frac{2}{\text{Re}}\nabla^2\omega = 0, \tag{6}$$

$$\nabla^2\psi = -\omega, \tag{7}$$

respectively. The boundary conditions eqns (3) and (4) are then expressed as

$$\psi = -\sin\theta, \quad \frac{\partial\psi}{\partial r} = -\sin\theta - \alpha, \qquad \text{on } r = 1, \quad 0 \leq \theta < 2\pi, \tag{8}$$

$$\frac{\partial\psi}{\partial r} = \frac{1}{r}\frac{\partial\psi}{\partial\theta} \to 0, \qquad \text{as } r \to \infty, \quad 0 \leq \theta < 2\pi. \tag{9}$$

3. Numerical Method

Filon [24] showed that the asymptotic form for the stream function at large distances from the cylinder and outside the wake region is given by

$$\psi \sim \frac{C_L \ln r}{2\pi} + \frac{C_D}{2\pi}(\theta - \pi), \quad r \to \infty, \quad 0 \leq \theta < 2\pi. \tag{10}$$

Since the stream function and vorticity equations are both elliptical in nature we should supply one condition for each of the variables rather than use directly conditions eqns (8) and (9). It has been reported that the choice of the boundary condition for the vorticity ω is not as sensitive as that for the stream function ψ (see, Refs [6] and [18]). Hence many authors have paid particular attention to the boundary condition for ψ at large distances from the cylinder. Because of the importance of the choice of the most appropriate boundary condition for ψ at large distances from the cylinder a method which avoids making this decision was introduced by Ingham and Tang [23] (see also, Ref. [25]). From the asymptotic expression eqn (10) we have

$$\psi/r \to 0 \quad \text{as} \quad r \to \infty, \quad 0 \leq \theta < 2\pi. \tag{11}$$

Hence we introduce the transformations

$$\xi = 1/r, \quad \eta = 2\theta/\pi, \quad f(r,\theta) = \psi(r,\theta)/r. \tag{12}$$

With the transformation eqn (12), the flow region ($1 \leq r < \infty, 0 \leq \theta < 2\pi$) is transformed into a finite rectangular region of the (ξ, η) plane ($0 \leq \xi \leq 1, 0 \leq \eta < 4$). Substituting from eqn (12) into eqns (6) and (7), we obtain

$$-\frac{2\xi^2}{\pi}\frac{\partial(f,\omega)}{\partial(\xi,\eta)} + \frac{2\xi}{\pi} f \frac{\partial \omega}{\partial \eta} + \xi^2 \frac{\partial \omega}{\partial \xi}\cos(\pi\eta/2) + \frac{2\xi}{\pi}\frac{\partial \omega}{\partial \eta}\sin(\pi\eta/2) + \frac{2}{\mathrm{Re}}\left[\xi^4 \frac{\partial^2 \omega}{\partial \xi^2} + \frac{4\xi^2}{\pi^2}\frac{\partial^2 \omega}{\partial \eta^2} + \xi^3 \frac{\partial \omega}{\partial \xi}\right] = 0, \tag{13}$$

$$\xi^3 \frac{\partial^2 f}{\partial \xi^2} + \frac{4\xi}{\pi^2}\frac{\partial^2 f}{\partial \eta^2} - \xi^2 \frac{\partial f}{\partial \xi} + \xi f = -\omega, \tag{14}$$

with $0 \leq \xi \leq 1, 0 \leq \eta < 4$. The boundary conditions eqns (8) and (9) become

$$f = -\sin(\pi\eta/2), \quad \partial f/\partial \xi = \alpha, \qquad \text{on } \xi = 1, \quad 0 \leq \eta < 4, \tag{15}$$

$$f = 0, \ \omega = 0, \qquad \text{on } \xi = 0, \quad 0 \leq \eta < 4, \tag{16}$$

and since the solution is periodic we also require that

$$f(\xi, 4) = f(\xi, 0), \quad \omega(\xi, 4) = \omega(\xi, 0), \quad 0 \leq \xi \leq 1. \tag{17}$$

In order to obtain numerical solutions of eqns (13)-(17), the region of integration $0 \leq \xi \leq 1$, $0 \leq \eta < 4$ is covered by a square mesh of size h and central finite difference approximations to the differential eqns (13) and (14) are employed. In practice, a mesh system is set up such that the mesh size in both the ξ and η directions is $h = 1/N$ where N is a preassigned positive integer. Full details of the resulting finite-difference equations and the methods of solution may be found in Ingham [18].

If L and D are the lift and drag on the cylinder, the lift and drag coefficients are defined by

$$C_L = L/2\rho U^2 a, \quad C_D = D/2\rho U^2 a, \tag{18}$$

and each consists of component due to the friction forces and the pressure. Hence

$$C_L = C_{LF} + C_{LP} = -\frac{2}{\mathrm{Re}}\int_0^{2\pi} (\omega)_{\xi=1}\cos\theta \, d\theta - \frac{2}{\mathrm{Re}}\int_0^{2\pi}\left(\frac{\partial \omega}{\partial \xi}\right)_{\xi=1}\cos\theta \, d\theta, \tag{19}$$

$$C_D = C_{DF} + C_{DP} = -\frac{2}{\mathrm{Re}}\int_0^{2\pi} (\omega)_{\xi=1}\sin\theta \, d\theta - \frac{2}{\mathrm{Re}}\int_0^{2\pi}\left(\frac{\partial \omega}{\partial \xi}\right)_{\xi=1}\sin\theta \, d\theta, \tag{20}$$

Formulae (19) and (20) are calculated by means of a second-order accurate finite-difference method and Simpson's rule.

4. Power series solution for small rotational parameter

To solve eqns (6) and (7) we assume expansions for ψ and ω as power of α in the form

$$\psi = \psi_0 + \alpha\psi_1 + \alpha^2\psi_2 + \cdots, \quad \text{i.e.} \quad f = f_0 + \alpha f_1 + \alpha^2 f_2 + \cdots \tag{21}$$

$$\omega = \omega_0 + \alpha\omega_1 + \alpha^2\omega_2 + \cdots \tag{22}$$

Subsituting eqns (21) and (22) into eqns (13) and (14) and equating coefficients of successive powers of α, the following equations are obtained

$$-\frac{2\xi^2}{\pi}\sum_{p=0}^{n}\frac{\partial(f_{n-p},\omega_p)}{\partial(\xi,\eta)} + \frac{2\xi}{\pi}\sum_{p=0}^{n} f_{n-p}\frac{\partial\omega_p}{\partial\eta} + \xi^2\frac{\partial\omega}{\partial\xi}\cos\left(\frac{\pi\eta}{2}\right) + \frac{2\xi}{\pi}\frac{\partial\omega_n}{\partial\eta}\sin\left(\frac{\pi\eta}{2}\right) + \frac{2}{\mathrm{Re}}\left[\xi^4\frac{\partial^2\omega_n}{\partial\xi^2} + \frac{4\xi^2}{\pi^2}\frac{\partial^2\omega_n}{\partial\eta^2} + \xi^3\frac{\partial\omega_n}{\partial\eta}\right] = 0, \tag{23}$$

and

$$\xi^3\frac{\partial^2 f_n}{\partial\xi^2} + \frac{4\xi}{\pi^2}\frac{\partial^2 f_n}{\partial\eta^2} - \xi^2\frac{\partial f_n}{\partial\xi} + \xi f_n = -\omega_n, \tag{24}$$

with $0 \le \xi \le 1, 0 \le \eta < 4$ and $n \ge 0$.

Using conditions eqns (15) and (16) the functions f_n and ω_n must satisfy

$$f_n = \left\{\begin{array}{ll} -\sin(\pi\eta/2) & \text{if } n = 0 \\ 0 & \text{if } n \neq 0 \end{array}\right\} \quad \text{on} \quad \xi = 1, \quad 0 \le \eta < 4, \tag{25a}$$

$$\frac{\partial fn}{\partial\xi} = \left\{\begin{array}{ll} 1 & \text{if } n = 1 \\ 0 & \text{if } n \neq 1 \end{array}\right\} \quad \text{on} \quad \xi = 1, \quad 0 \le \eta < 4, \tag{25b}$$

$$f_n = 0, \quad \text{on} \quad \xi = 0, \quad 0 \le \eta < 4, \tag{26a}$$

$$\omega_n = 0, \quad \text{on} \quad \xi = 0, \quad 0 \le \eta < 4. \tag{26b}$$

Subsituting eqn (22) into eqns (19) and (20), we obtain

$$C_{DF} = C_{DF}^{(0)} + \alpha C_{DF}^{(1)} + \alpha^2 C_{DF}^{(2)} + \cdots = -\frac{2}{\mathrm{Re}}\sum_{n=0}^{\infty}\int_0^{2\pi}(\omega_n)_{\xi=1}\sin\theta\,d\theta, \tag{27a}$$

$$C_{LF} = C_{LF}^{(0)} + \alpha C_{LF}^{(1)} + \alpha^2 C_{LF}^{(2)} + \cdots = -\frac{2}{\mathrm{Re}}\sum_{n=0}^{\infty}\int_0^{2\pi}(\omega_n)_{\xi=1}\cos\theta\,d\theta, \tag{27b}$$

$$C_{DP} = C_{DP}^{(0)} + \alpha C_{DP}^{(1)} + \alpha^2 C_{DP}^{(2)} + \cdots = -\frac{2}{\mathrm{Re}}\sum_{n=0}^{\infty}\int_0^{2\pi}\left(\frac{\partial\omega_n}{\partial\xi}\right)_{\xi=1}\sin\theta\,d\theta, \tag{28a}$$

$$C_{LP} = C_{LP}^{(0)} + \alpha C_{LP}^{(1)} + \alpha^2 C_{LP}^{(2)} + \cdots = -\frac{2}{\mathrm{Re}}\sum_{n=0}^{\infty}\int_0^{2\pi}\left(\frac{\partial\omega_n}{\partial\xi}\right)_{\xi=1}\cos\theta\,d\theta, \tag{28b}$$

and finally, C_D and C_L can then be evaluated using

$$C_D = C_D^{(0} + \alpha C_D^{(1)} + \alpha^2 C_D^{(2)} + \cdots, \tag{29}$$

$$C_D = C_L^{(0} + \alpha C_L^{(1)} + \alpha^2 C_L^{(2)} + \cdots. \tag{30}$$

TABLE 1. Values of the drag coefficients C_D estimated from various mesh sizes for Re $= 60$ and Re $= 100$ with $\alpha = 0$

	Re $= 60$			Re $= 100$		
	C_{DP}	C_{DF}	C_D	C_{DP}	C_{DF}	C_D
(i)	0.896	0.398	1.294	0.806	0.288	1.094
(ii)	0.885	0.397	1.282	0.783	0.283	1.066
(iii)	0.882	0.397	1.279	0.777	0.282	1.059
(iv)	0.882	0.397	1.279	0.777	0.282	1.059

The rows (i)-(iii) give the numerical results for $h = 1/15$, $1/20$ and $1/30$, respectively. Row (iv) is the repeated h^2-extrapolant obtained from (i)-(iii).

5. NUMERICAL RESULTS

The results for Re $= 60$ and 100 and $\alpha = 0, 0.1, 0.5$ and 1 with mesh size $h = 1/15$, 1/20 and 1/30 have been obtained. All the final results presented have been obtained using repeated h^2-extrapolation for each value of Re and α.

In order to check the accuracy the case of no rotation is compared with the results obtained by previous investigators to this problem. It is found that the contour lines for the stream function, pressure and vorticity distribution on the surface of the cylinder in the case of $\alpha = 0$ are in good agreement with most of the previous investigators (see, e.g. Refs [6, 7] and [9]). Table 1 shows the variation of C_{DP}, C_{DF}, and C_d for Re $= 60$ and 100 in the case of no rotation and the h^2-extrapolation results. The most accurate results of Fornberg [6] suggest that $C_D = 1.058$ at Re $= 100$ and this should be compared with the present result of $C_D = 1.059$. Dennis and Chang [9] obtained that $C_{DF} = 0.282$ and $C_{DP} = 0.774$ at Re $= 100$ whilst the present results give $C_{DF} = 0.282$ and $C_{DP} = 0.777$. The obtained length of the wake bubble for Re $= 100$ is 13.1 which is in reasonable

TABLE 2. The series expansion results

	$C_{DP}^{(0)}$	$C_{DF}^{(0)}$	$C_D^{(0)}$	$C_{LP}^{(1)}$	$C_{LF}^{(1)}$	$C_L^{(1)}$	$C_{DP}^{(2)}$	$C_{DF}^{(2)}$	$C_P^{(2)}$
(i)	0.896	0.398	1.294	1.681	0.180	1.861	0.020	0.025	0.045
(ii)	0.885	0.397	1.282	1.805	0.190	1.995	-0.016	0.021	0.005
(iii)	0.882	0.397	1.279	1.901	0.192	2.093	-0.049	0.020	-0.029
(iv)	0.882	0.397	1.279	1.981	0.191	2.172	-0.08	0.02	-0.06

Values of the lift coefficients C_L and the drag coefficients C_D estimated from various mesh sizes for Re $= 60$ (see Table 1).

TABLE 3. The series expansion results

	$C_{DP}^{(0)}$	$C_{DF}^{(0)}$	$C_D^{(0)}$	$C_{LP}^{(1)}$	$C_{LF}^{(1)}$	$C_L^{(1)}$	$C_{DP}^{(2)}$	$C_{DF}^{(2)}$	$C_P^{(2)}$
(i)	0.806	0.288	1.094	1.528	0.142	1.670	0.025	0.020	0.045
(ii)	0.783	0.283	1.066	1.622	0.142	1.764	0.005	0.022	0.027
(iii)	0.777	0.282	1.059	1.681	0.141	1.822	-0.035	0.023	-0.012
(iv)	0.777	0.282	1.059	1.723	0.140	1.863	-0.07	0.02	-0.05

Values of the lift coefficients C_L and the drag coefficients C_D estimated from various mesh sizes for Re $= 100$ (see Table 1).

TABLE 4. Variation of C_L and C_D with α for Re $= 60$ and 100 as obtained by the full Navier-Stokes solution (N.S.) and the series expansion solution (SE)

	Re $= 60$				Re $= 100$			
	C_L		C_D		C_L		C_D	
α	N.S.	SE	N.S.	SE	N.S.	SE	N.S.	SE
0	0.000	0.000	1.279	1.279	0.000	0.000	1.058	1.058
0.1	0.212	0.217	1.274	1.278	0.179	0.186	1.054	1.057
0.5	1.109	1.085	1.251	1.264	0.955	0.930	1.030	1.044
1	2.249	2.170	1.207	1.219	1.973	1.860	0.983	1.008

agreement with the value of 14.11 as obtained by Dennis and Chang [9], 12.0 by Ta Phuoc Loc [17], and 13.7 by Fornberg [6].

An investigation of eqns (23) and (24) subject to the boundary conditions (25) and (26) gives

$$C_{LF}^{(m)} = C_{LP}^{(m)} = C_{L}^{(m)} \equiv 0, \quad \text{for } m \text{ an even positive integer,} \tag{31a}$$

and

$$C_{DF}^{(m)} = C_{DP}^{(m)} = C_{D}^{(m)} \equiv 0, \quad \text{for } m \text{ an odd positive integer,} \tag{31b}$$

Tables 2 and 3 show the variation of C_{LP}, C_{LF}, C_L, C_{DP} and C_D up to second order terms for Re $=$ 60 and 100, respectively, and the repeated h^2-extrapolation results. The final extrapolated results suggest that

$$\left.\begin{array}{rcl} C_{LP} & \sim & 1.98\alpha + 0(\alpha^3), \\ C_{LF} & \sim & 0.19\alpha + 0(\alpha^3), \\ C_L & \sim & 2.17\alpha + 0(\alpha^3); \end{array}\right\} \quad \text{for Re } = 60, \tag{32a}$$

$$\left.\begin{array}{rcl} C_{LP} & \sim & 1.72\alpha + 0(\alpha^3), \\ C_{LF} & \sim & 0.14\alpha + 0(\alpha^3), \\ C_L & \sim & 1.86\alpha + 0(\alpha^3); \end{array}\right\} \quad \text{for Re } = 100, \tag{32b}$$

$$\left.\begin{array}{rcl} C_{DP} & \sim & 0.882 - 0.08\alpha^2 + 0(\alpha^3), \\ C_{DF} & \sim & 0.397 + 0.02\alpha^2 + 0(\alpha^3), \\ C_D & \sim & 1.279 - 0.06\alpha^2 + 0(\alpha^3); \end{array}\right\} \quad \text{for Re } = 60, \tag{32c}$$

$$\left.\begin{array}{rcl} C_{DP} & \sim & 0.777 - 0.07\alpha^2 + 0(\alpha^3), \\ C_{DF} & \sim & 0.282 + 0.02\alpha^2 + 0(\alpha^3), \\ C_D & \sim & 1.059 - 0.05\alpha^2 + 0(\alpha^3); \end{array}\right\} \quad \text{for Re } = 100, \tag{32d}$$

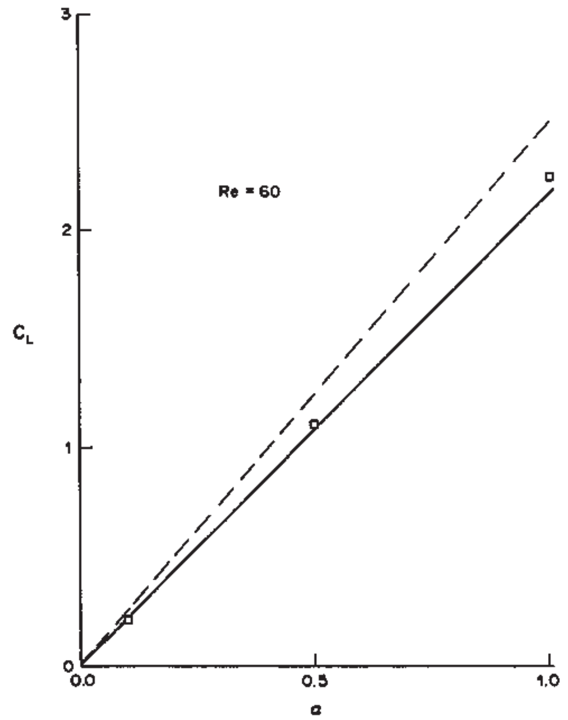

FIG. 1. Variation of C_L with α for Re $= 60$: $\square$, numerical solutions of the Navier-Stokes equations; ——, series expansion solutions; – – –, the results obtained by Badr *et al.* (1989).

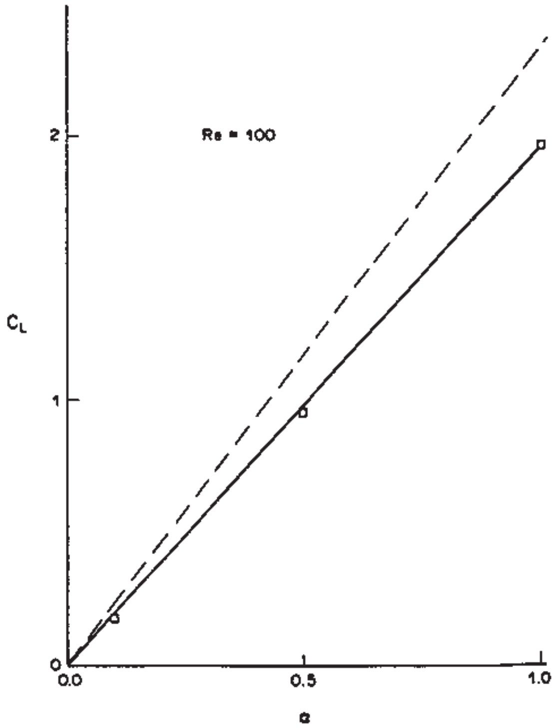

FIG. 2. Variation of C_L with α for Re $= 100$: $\square$, numerical solutions of the Navier-Stokes equations; ——, series expansion solutions; – – –, the results obtained by Badr *et al.* (1989).

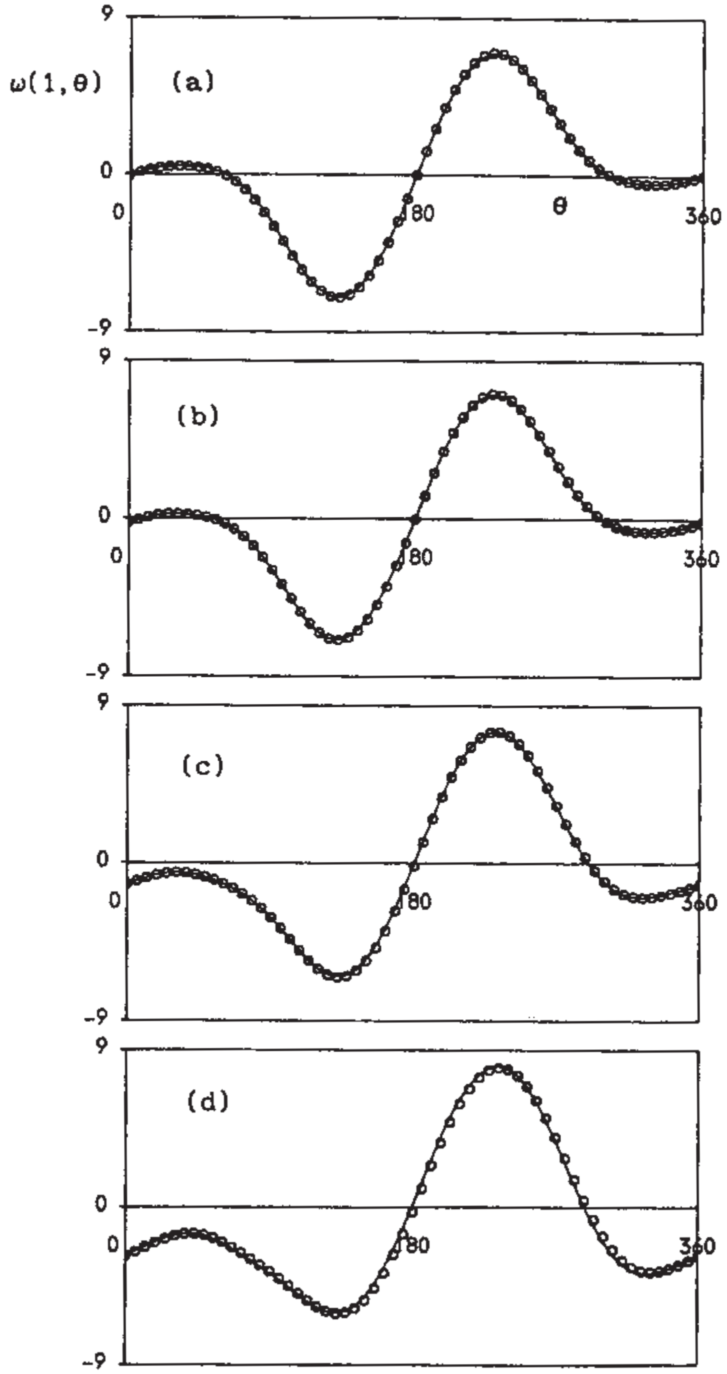

FIG. 3. Mesh size influence on the surface vorticity for Re $= 60$ and (a) $\alpha = 0$, (b) $\alpha = 0.1$, (c) $\alpha = 0.5$ and (d) $\alpha = 1$ with $h = 1/15$ (◯ ◯ ◯) and $1/30$ (——).

The values of C_D and C_L as obtained by solving the full Navier-Stokes equations are given in Table 4 for Re $= 60$ and 100. The values quoted in this table have again been obtained by using repeated h^2-extrapolation and the results are quite accurate (at most 3% in error). Also shown in Table 4 are the corresponding values as obtained using the series solution for small values of α as given in eqns (32). It is observed that range of validity of the series results given in eqns (32) is quite large with results at $\alpha = 1$ being at most in error by about 6%.

Figure 1 and 2 show the variation of C_L as obtained by solving the full Navier-Stokes equations for Re $= 60$ and 100, respectively, and $0 \leq \alpha \leq 1$. Also shown are the series expansion results as given in eqns (32). The agreement between the full numerical solution and the series solution is good.

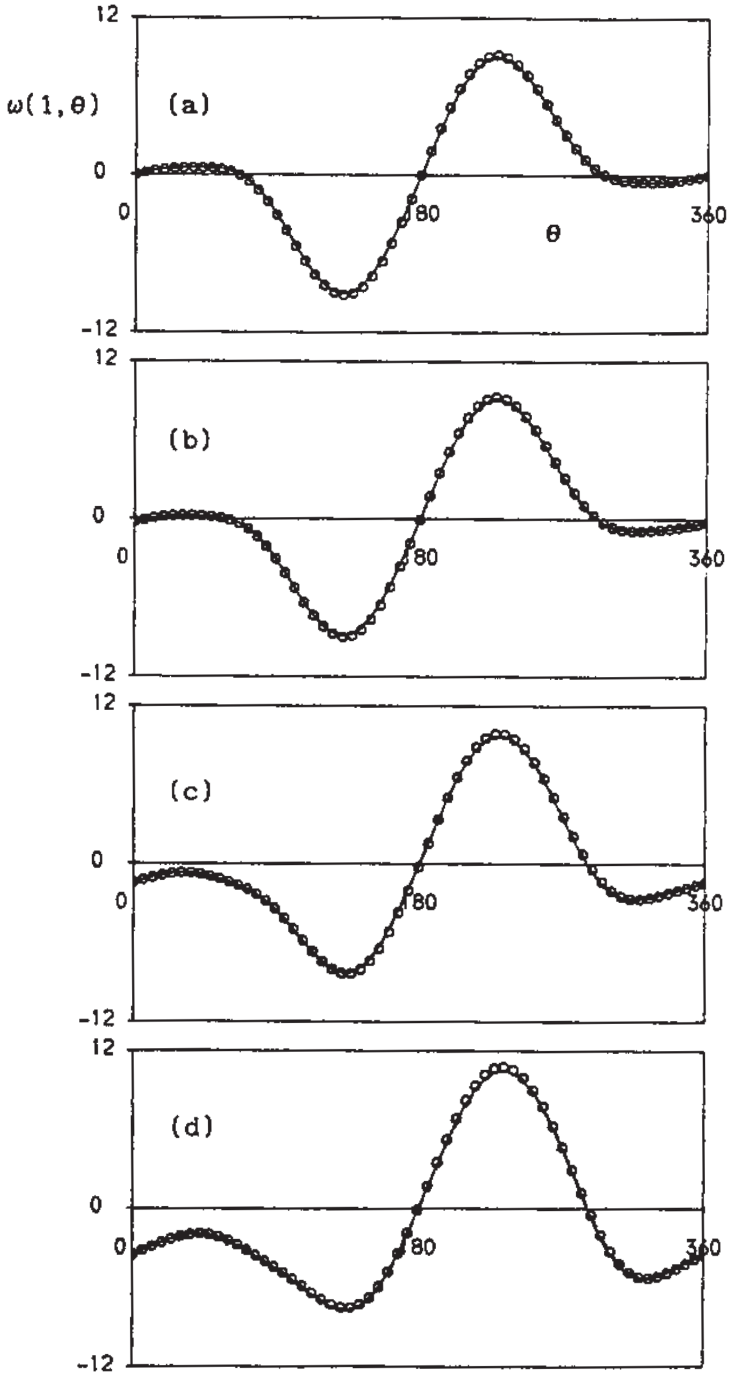

FIG. 4. Mesh size influence on the surface vorticity for Re $= 100$ and (a) $\alpha = 0$, (b) $\alpha = 0.1$, (c) $\alpha = 0.5$ and (d) $\alpha = 1$ with $h = 1/15$ (◯ ◯ ◯) and $1/30$ (——).

In the case of Re ≥ 60, the periodic variation with time of C_L was given by Badr *et. al.* [16] and an average value of C_L per complete cycle was calculated. It is observed that these average values are directly proportional to al and they are in reasonable agreement with the present results. It is seen that the results of Badr *et al.* [16] are a little higher and an average value of C_L per complete cycle was calculated. It is observed that these average values are directly proportional to α and they are in reasonable agreement with the present results. It is seen that the results of Badr *et al.* [16] are a little higher than those given by the present calculations and it is perhaps relevant to point out that, in the cases if Re $= 5$ and 20, the lift coefficients estimated by Badr *et al.* [16] are also a little higher than

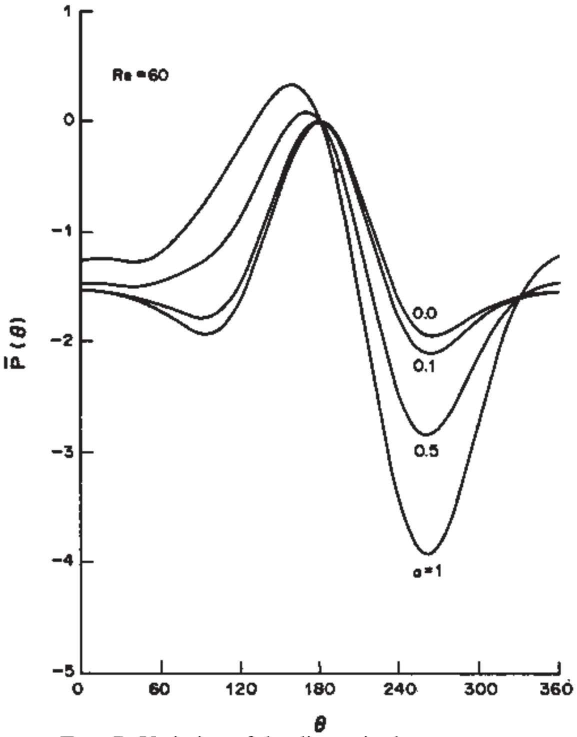

FIG. 7. Variation of the dimensionless pressure coefficient over the surface of the cylinder for Re $= 60$ and $\alpha = 0, 0.1, 0.5$ and 1.

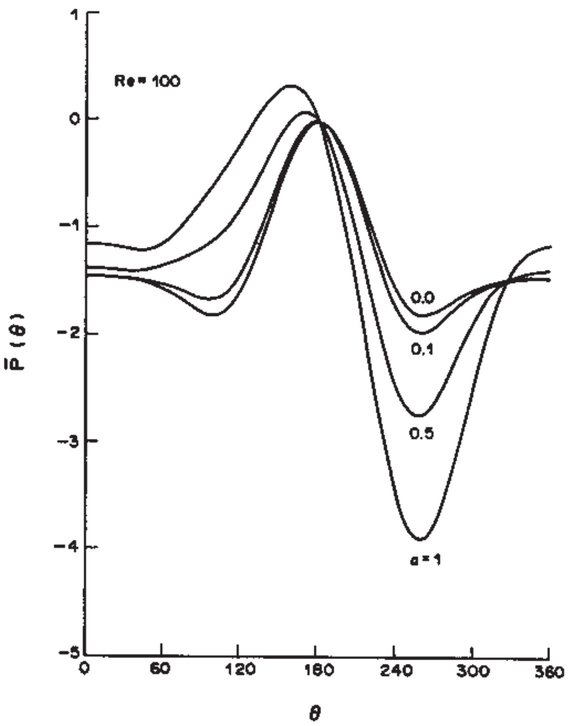

FIG. 8. Variation of the dimensionless pressure coefficient over the surface of the cylinder for Re $= 100$ and $\alpha = 0, 0.1, 0.5$ and 1.

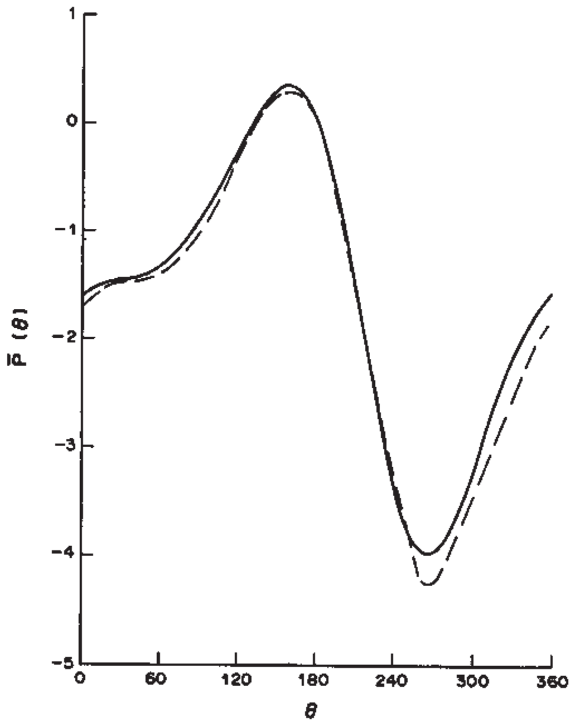

FIG. 9. Comparison of the dimensionless pressure coefficient on the surface of the cylinder for Re $= 20$ and $\alpha = 1$. —— Present solution, – – – Badr *et al.* solution.

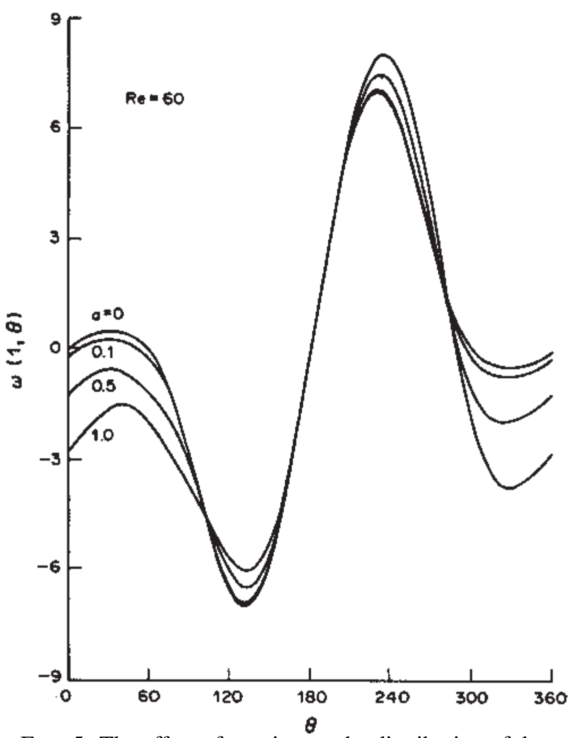

FIG. 5. The effect of rotation on the distribution of the surface vorticity with Re $= 60$.

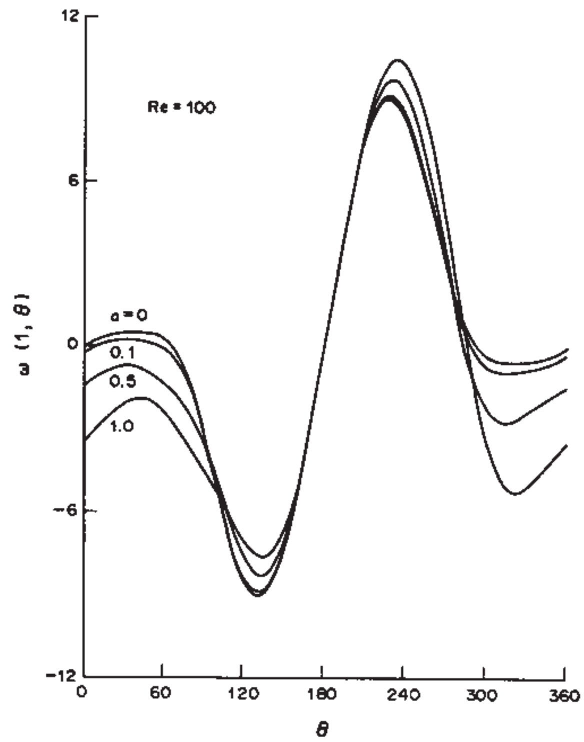

FIG. 6. The effect of rotation on the distribution of the surface vorticity with Re $= 100$.

those obtained by all of the previous investigators and it does not seem possible to give a reason for the discrepancies in these results.

To illustrate the mesh size influence, Figs 3 and 4 show the variation of the surface vorticity for Re $= 60$ and 100, respectively, with $h = 1/5$ and $1/30$, and $\alpha = 0, 0.1, 0.5$ and 1. Again, it is seen that the surface vorticity with the two mesh sizes are graphically very similar for $\alpha \leq 1$. Figures 5 and 6 show the effect of rotation on the distribution of surface vorticity for $0 \leq \alpha \leq 1$ and with Re $= 60$ and 100, respectively. In Fig. 6, at $\alpha = 0$, the results presented here are graphically indistinguishable from those given by Dennis and Chang [9] and Fornberg [6]. It is seen that the peak values of the vorticity on the upper surface ($0 < \theta < \pi$) and lower surface ($\pi < \theta < 2\pi$) of the cylinder increases slightly with increasing α for both Re $= 60$ and 100. Badr *et al.* [16] reached the same conclusion in the case of Re $= 20$ but Ingham [18] gave an opposing view for the upper surface.

It is seen from eqns (32) that greatest contribution to the lift coefficient is given by the pressure forces C_{LP}, approximately 91% for Re $= 60$ and 92% for Re $= 100$. The results of Ref. [23] suggest that the contribution of C_{LP} to C_L is about 80% at Re $= 5$ and 87% at Re $= 20$. It is interesting to note that the contribution of the pressure force to the lift force increases as the Reynolds number increases, although the rate of increase becomes smaller as a increases. This is in good agreement with the results given by Lyul'ka [15] who investigated the low Reynolds number cases of Re $= 2, 10, 15$ and 20. Further, it is observed that the values of C_{DP} and C_D decrease as α increases for both values of Re considered in this work whereas the contrary is true for C_{DF}.

Since in a viscous fluid a large part of the lift force is due to the pressure force, it is interesting to consider the contribution of the pressure on the surface of the cylinder. Figures 7 and 8 show the variation of the dimensionless pressure coefficient

$$\bar{P}(\theta) = [P^*(1, \theta) - P^*(1, \pi)]/(1/2\rho U^2), \tag{33}$$

over the surface of the cylinder for Re $= 60$ and 100 with $0 \leq \alpha \leq 1$, respectively, where P^* is the dimensional pressure on the cylinder. The non-dimensional θ component of the Navier-Stokes equations on the cylinder reduces to

$$\frac{\partial \bar{P}}{\partial \theta} = \frac{4}{\text{Re}} \left(\frac{\partial \omega}{\partial \xi} \right)_{\xi=1}. \tag{34}$$

Figure 9 shows the variation of the pressure coefficient over the surface of the cylinder for Re $= 20$ and $\alpha = 1$ obtained by the present calculation and by Badr et al. [16]. It is observed that there is certainly qualitative agreement between the two curves but the peak value on the lower surface ($\pi < 0 < 2\pi$) given by Badr *et al.* is a little lower than that given by present calculation. This is because the vorticity is very sensitive to the rotational parameter α near $\theta = 5\pi/3$ (see Figs 5 and 6) and thus the pressure coefficient changes rapidly with α on the lower surface of the cylinder.

Figures 10 and 11 show the contours of streamline and vorticity for Re $= 60$ and $\alpha = 0, 0.1, 0.5$ and 1, respectively. As expected the effect of rotation is to change substantially the streamline pattern near the surface of the cylinder. In the potential flow problem closed streamlines near the cylinder will only exist if $\alpha > 0.5$ but in the case of viscous flow closed streamlines will always exist for all non-zero values of α. These streamlines only exist very close to the cylinder for small values of α but as α increases they exist in larger and larger regions. An interesting discussion of the separation from a moving surface, similar to the present problem, is given in Elliott, Cowley and Smith [25]. Figure 10(d) shows a closed streamline for Re $= 60$ and $\alpha = 1$. For $\alpha < 1$ closed streamlines have found but they exist so close to the cylinder that it is difficult to plot them so that they are distinguishable from the surface of the cylinder. It is observed from Fig. 10 that the stream pattern becomes more asymmetrical about $\theta = 0$ as α increases. At $\alpha = 0.1$, $\psi = 0$ is no longer a closed streamline of

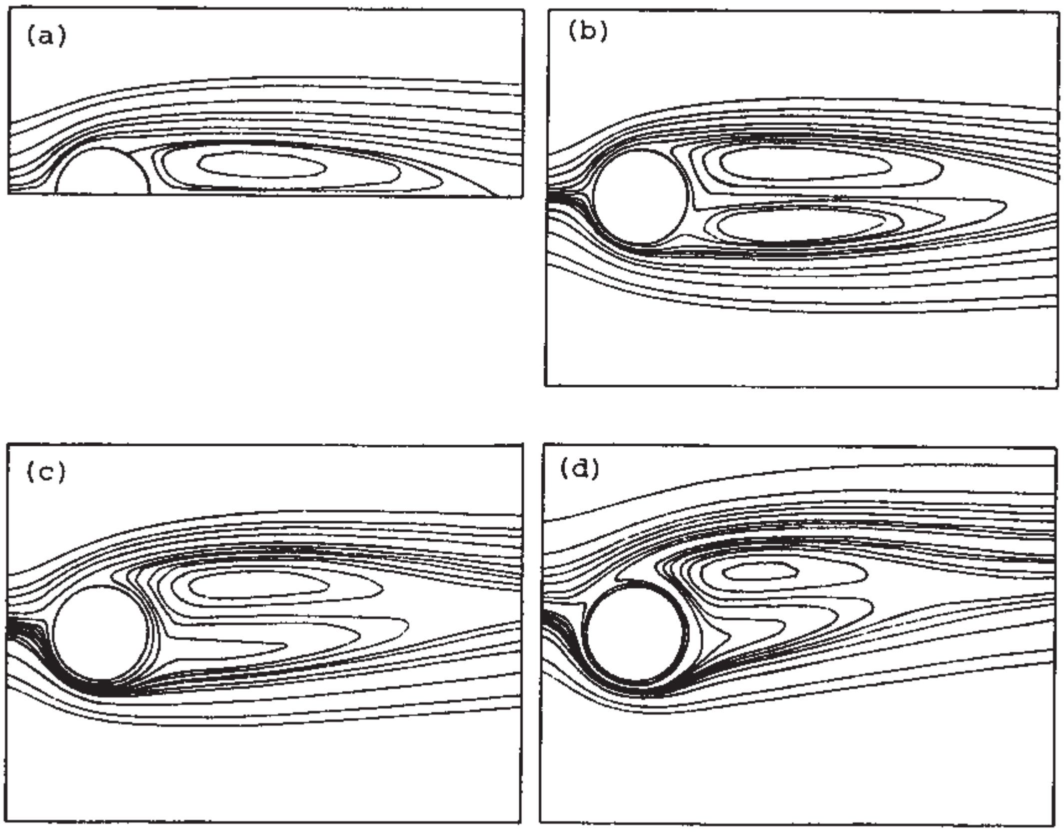

FIG. 10. Streamlines for Re $= 60$ and (a) $\alpha = 0$, the values of streamline are $1, 0.8, 0.5, 0.3, 0.2, 0.1, 0.05, 0, -0.01, -0.02, -0.05$; (b) $\alpha = 0.1$, the values of streamline are $0.5, 0.3, 0.2, 0.1, 0.05, 0, -0.01, -0.03, -0.05, -0.07, -0.1, -0.2, -0.3, -0.5, -0.8, -1$; (c) $\alpha = 0.5$, the values of streamline are $0.5, 0.3, 0.2, 0.1, 0, -0.05, -0.08, -0.1, -0.13, -0.15, -0.18, -0.2, -0,25, -0.3, -0.5, -0.8, -1$; and (d) $\alpha = 1$, the values of streamline are $1, 0.5, 0.3, 0.2, 0.1, 0, -0.05, -0.1, -0.2, -0.23, -0.25, -0.28, -0.3, -0.325, -0.35, -0.4, -0.5, -0.8, -1$.

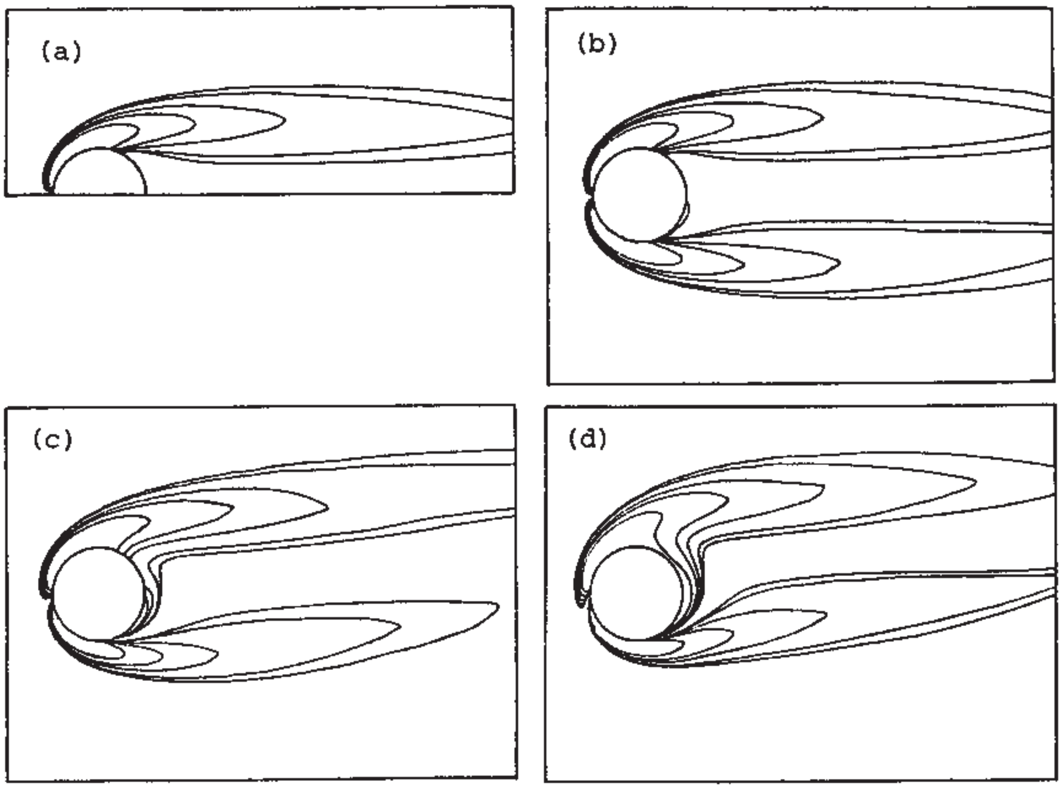

FIG. 11. Vorticity contours for Re $= 60$ and (a) $\alpha = 0$, (b) $\alpha = 0.1$, (c) $\alpha = 0.5$ and (d) $\alpha = 1$. Contour levels are -1.5, -1, -0.75, -0.5, -0.4, 0.4, 0.5, 0.75, 1, 1.5.

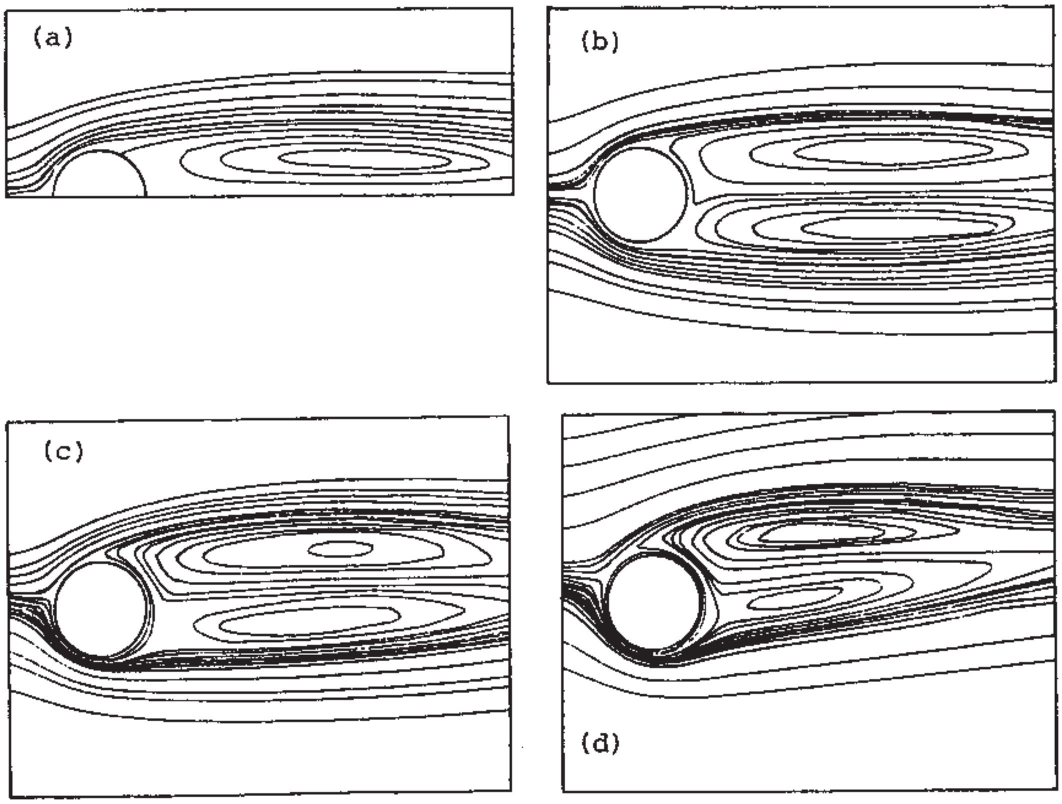

FIG. 12. Streamlines for Re $= 60$ and (a) $\alpha = 0$, the values of streamline are $1, 0.8, 0.5, 0.3, 0.2, 0.1, 0.05, 0, -0.05, -0.08, -0.1$; (b) $\alpha = 0.1$, the values of streamline are $1, 0.5, 0.2, 0.1, 0.07, 0.05, 0.02, 0, -0.05, -0.1, -0.12, -0.2, -0.3, -0.4, -0.5, -0.8, -1, -1.5$; (c) $\alpha = 0.5$, the values of streamline are $0.5, 0.3, 0.2, 0.1, 0, -0.01, -0.04, -0.06, -0.1, -0.12, -0.15, -0.18, -0.2, -0.23, -0.25, -0.3, -0.5, -0.8, -1, -1.5$; and (d) $\alpha = 1$, the values of streamline are $2, 1.5, 1, 0.5, 0, -0.05, -0.1, -0.16, -0.18, -0.2, -0.24, -0.27, -0.3, -0.31, -0.32, -0.35, -0.5, -1, -1.5$.

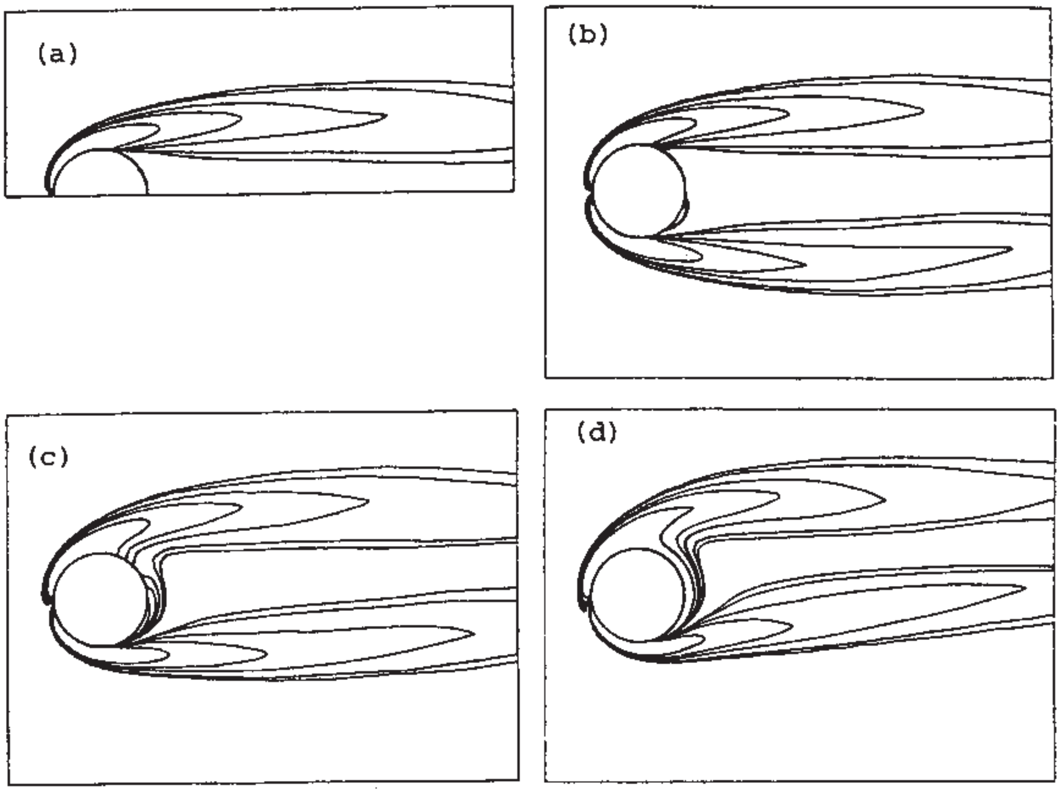

FIG. 13. Vorticity contours for Re = 100 and (a) $\alpha = 0$, (b) $\alpha = 0.1$, (c) $\alpha = 0.5$ and (d) $\alpha = 1$. Contour levels are $-1.5, -1, -0.75, -0.5, -0.4, 0.4, 0.5, 0.75, 1, 1.5$.

upper bubble but is still a closed streamline of lower bubble. The upper and lower bubbles become smaller as α increases while the lower one vanishes as $\alpha \geq 0.5$.

Figures 12 and 13 show the contours of streamline and vorticity for Re $= 100$ with $\alpha = 0, 0.1, 0.5$ and 1, respectively. The streamline pattern at $\alpha = 0$ is in good agreement with those of Dennis and Chang [9] and Fornberg [6]. Again as α increases the region of the wake bubble becomes smaller and the lower wake eddy is smaller than the upper one when $\alpha > 0$. It can be expected that the lower wake bubble will vanish at a certain value $\alpha > 1$.

REFERENCES

[1] I. Imai, On the asymptotic behaviour of viscous fluid flow at a great distance from a cylinderical body. *Proc. R. Soc.* **A208**, 487 (1951).
[2] M. Kawaguti, Numerical solution of the Navier-Stokes equations for the flow around a circular cylinder at Reynolds number 40. *J. Phys. Soc. Jap*. **8**, 747 (1953).
[3] D. W. Moore, The flow past a rapidly rotating circular cylinder in a infinite stream. *J. Fluid Mech*. **2**, 541 (1957).
[4] F. T. Smith, Laminar flow of an incompressible fluid past a bluff body: the separation, reattachment, eddy properties and drag. *J. Fluid Mech.* **92**, 171 (1979).
[5] F. T. Smith, A structure for laminar flow past a bluff body at high Reynolds number. *J. Fluid Mech*. **155**, 175 (1985).
[6] B. Fornberg, A numerical study of steady viscous flow past a circular cylinder. *J. Fluid Mech*. **97**, 819 (1980).
[7] B. Fornberg, Steady viscous flow past a circular cylinder up to Reynolds number 600. *J. Comput. Phys*. **61**, 297 (1985).
[8] H. M. Badr and S. C. R. Dennis, Time-dependent viscous flow past an impulsively started rotating and translating circular cylinder. *J. Fluid Mech*. **158**, 447 (1985).
[9] S. C. R. Dennis and G. Z. Chang, Numerical solutions for steady flow past a circular cylinder at Reynolds numbers up to 100. *J. Fluid Mech.* **42**, 471 (1970).
[10] J. S. Tennant, W. S. Johnson and A. Krothapalli, Rotating cylinder for circulation control on an aerofoil. *J. Hydronaut*. **10**, 102 (1976).
[11] A. T. Sayers, Lift coefficient and flow visualization on a leading edge rotating cylinder rudder. *Int. J. Mech. elect. Engng* **7**, 75 (1979).

[12] D. C. Thoman and A. A. Saewczyk, Numerical solutions of time-dependent two-dimensional flow of a viscous incompressible fluid over stationary and rotating cylinders. Dept of Mech. Engng, University of Notre Dame, Tech. Report 66-14 (1966).
[13] W. M. Swanson, Report, Dept. of Mech. Engng. Case Institute of Technology.
[14] L. Prandtl and O. G. Tietjens. *Applied Hydro- and Aeromechanics*. McGraw-Hill, New York. (1934).
[15] V. A. Lyul'ka, Numerical solution of the problem of the rotation of a cylinder in a flow of viscous incompressible fluid. *Zh. vychisl. Mat. mat. Fiz*. **17**, 470 (1970).
[16] H. M. Badr, S. C. R. Dennis and P. J. S. Young, Steady and unsteady flow past a rotating circular cylinder at low Reynolds numbers. *Comput. Fluids* **17**, 579 (1989).
[17] P. L. Ta, Étude numérique de l'écoulement d'un fluide visqueux incompressible autour d'un cylindre fixe ou en rotation. Effet Magnus. *J. Méc*. **14**, 109 (1975).
[18] D. B. Ingham, Steady flow past a rotating cylinder. *Comput. Fluids* **11**, 351 (l983).
[19] M. B. Glauert, The flow past a rapidly rotating circular cylinder. *Proc. R. Soc. Lond*. **A230**, l08 (1957).
[20] M. B. Glauert, A boundary layer theorem, with applications to rotating cylinders. *J. Fluid. Mech*. **2**, 89 (l957b).
[21] W. W. Wood, Boundary layers whose streamlines are closed. *J. Fluid Mech*. **2**, 77 (l957).
[22] S. C. R. Dennis, The computation of two-dimensional asymmetrical flows past cylinders. *Comput. Fluid. Dynam., SIAM-AMS Proc.* **11**, 156 (1978).
[23] D. B. Ingham and T. Tang, A numerical investigation into the steady past a rotating circular cylinder at low and intermediate Reynolds numbers, *J. Comput. Phys*. **87**, 91 (1990).
[24] L. N.G. Filon, The forces on a cylinder in a stream of viscous fluid *Proc. R. Soc.* **A113**, 7 (1926).
[25] T. Tang, Numerical solutions of the Navier-Stokes Equations, Ph.D. Thesis, University of Leeds (1989).
[26] J. W. Elliot, S. J. Cowley and F. T. Smith, Breakdown of boundary layers: (i) on moving surfaces; (ii) in semi-similar unsteady flow; (iii) in fully unsteady flow. *Geophys. Astrophys. Fluid Dynam.* **25**, 77 (1983).